CrystEngComm

Cite this: *CrystEngComm*, 2011, **13**, 4491

www.rsc.org/crystengcomm

COMMUNICATION

In situ studies of different growth modes of silver crystals induced by the concentration field in an aqueous solution†

Hongjun You,[a] Chunhua Ding,*[b] Xiaoping Song,[c] Bingjun Ding[ac] and Jixiang Fang*[c]

Received 6th March 2011, Accepted 20th April 2011
DOI: 10.1039/c1ce05289f

An *in situ* observation of silver hierarchical crystal growth in a Zn/$AgNO_3$ (aq.) replacement reaction system revealed that the morphological evolution of silver crystal strongly depended on the change of the silver ion concentrations. With the increasing concentration, the morphologies of the silver crystal transformed from loose fractal (LF) to dense branch morphology (DBM) and even to dendrite. The concentration field was *in situ* monitored using a Michelson interferometer during the reaction and the profile of the concentration field was studied based on experimental observation. The crystals morphology transform was induced by different growth modes. At low concentration, the growth mode was ion diffusion limited growth and at the high concentration the growth mode was protuberant growth which was decided by reaction limitation.

Metal nanocrystals have attracted great interest due to their fundamental size- and shape-dependent properties for many important potential technological applications.[1] Hierarchical metal nanocrystals, such as fractal and dendritic nanocrystals, due to their higher structural complexity compared to nanoparticles, nanowires and nanoplates, are expected to have a wide range of technological applications, such as interconnections in the bottom-up self-assembly of nanocircuits and nanodevices.[2] Pd–Pt, Au–Pt and PtAu bimetallic nanodendrites have been synthesized using seed growth methods and shown excellent catalytic properties for oxygen reduction reaction (ORR) and formic acid oxidation reaction in a proton-exchange membrane (PEM) fuel cell.[3–5] The applications of hierarchical metal nanocrystal for surface-enhanced Raman scattering (SERS),[6] electrochemistry or photo-catalysts,[7] and left-handed materials (LHMs)[8] have been widely exploited and studied.

Many methods have been developed to synthesize hierarchical metal nanocrystals, such as electrochemical deposition,[9,10] galvanic replacement,[11–13] reducing of metal precursors by tetrathiafulvalene[14] or ascorbic acid,[15] ultrasonically assisted templated synthesis,[2] ultraviolet irradiation photoreduction,[16] plating,[17] γ-irradiation route,[18] and pulsed sonoelectrochemical methods.[19] Understanding of nucleation and growth mechanisms is a prerequisite for the shape controlling of hierarchical metal nanocrystals. However, up to now, the intrinsic mechanism of metal hierarchical nanocrystal growth in solution is still not very clear. It is commonly recognized that the metal hierarchical nanostructure is formed at non-equilibrium conditions and many factors have been studied how to affect metal hierarchical nanostructure formation, including convection,[20] ion concentration,[21] voltage in electrodeposition,[22] surfactant agent,[23–25] crystalline anisotropy,[26] competition between thermodynamic and kinetic,[27] temperature,[23,28] *etc.* Based on a diffusion-limited aggregation (DLA) model,[29] hierarchical crystals with fractal morphology were simulated and their morphology transforms have been successfully explained with a computer simulation model. In the DLA model, the shape transformation is explained by competition of anisotropy and random diffusion of building unit.[17] When the anisotropy effect becomes stronger over random, the hierarchical shape transforms from loose fractal (LF) to dense branch morphology (DBM).[30] The theory is only built on computer simulation, but the mechanism of real hierarchical shape transform in experiment is still not explained with theory very well.

Recently, *in situ* observation was developed to study the hierarchical crystals growth. Using *in situ* transmission electron microscopy (TEM), it was observed that platinum nanocrystals could grow either by monomer attachment from solution or by particle coalescence, and dendritic nanostructures would be formed by particles aggregation.[31] The aggregated nanoparticles would be perfectly aligned under oriented attachment (OA) mechanism[32–34] to form hierarchical mesoscale structures.[35] *In situ* synchrotron-based X-ray diffraction (XRD) was also used to study the mechanism of hierarchical dendritic platinum nanocrystal formation.[36] Here using a Michelson interferometer, we *in situ* monitored the concentration profiles near silver hierarchical crystals. The result shows that the concentration profiles near the reaction interface have an important effect on silver hierarchical crystals growth. Based on experimental observation, two different growth modes induced by different concentration profiles were developed to explain the mechanism of shape transformation.

In our experiment a basic and simple method of galvanic replacement was used to study the effect of concentration field on silver hierarchical nanostructure growth. The galvanic replacement

[a]*Materials Science and Engineering School, State Key Laboratory for Mechanical Behavior of Materials, Xi'an Jiaotong University, Shannxi, 710049, PR China*
[b]*School of Aerospace, Xi'an Jiaotong University, Shann Xi, 710049, PR China. E-mail: chding@mail.xjtu.edu.cn*
[c]*School of Science, MOE Key Laboratory for Non-Equilibrium Synthesis and Modulation of Condensed Matter, Xi'an Jiaotong University, Shannxi, 710049, PR China. E-mail: jxfang@mailst.xjtu.edu.cn*

† Electronic supplementary information (ESI) available: Details of experiments; schematic sketch of experimental equipment (Fig. S1), TEM images, EDX and XRD patterns of product (Fig. S2–S4). See DOI: 10.1039/c1ce05289f

reaction has been widely used to study metal nanostructure growth[12,13,37] and also has been used to synthesize Au, Pt or Pd hollow nanostructures with a range of different shapes (*e.g.* triangular rings, prism-shaped boxes, cubic boxes, spherical capsules, and tubes).[38] The details of experiment are described in the ESI† (Experimental section and Fig. S1). In silver nitrate aqueous solution, silver ions were reduced to silver atoms by zinc atoms through galvanic replacement reaction and silver atoms were deposited and aggregated on a zinc plate to form fractal or dendritic hierarchical crystals. The chemical reactions as well as redox potentials are shown as the following equations:

$$Zn \rightarrow Zn^{2+} + 2e \ (E^0Zn/Zn^{2+} = -0.762 \text{ V}) \quad (1)$$

$$Ag^+ + e \rightarrow Ag \ (E^0Ag/Ag^+ = 0.799 \text{ V}) \quad (2)$$

The growth of silver hierarchical crystal was *in situ* observed using optic microscopy. Fig. 1a–c show the optical micrographs of fractal or dendritic silver trees prepared at silver ion concentrations of 30 mM, 100 mM, and 200 mM respectively. The corresponding reaction times were 360 s, 80 s and 30 s. A series of concentrations from low to high were investigated using this method and the morphological transform was found as Fig. 1d shows. There are three typical morphologies obtained with the concentration increasing from 1 mM to 300 mM. These typical morphologies are loose fractal trees (LF, Fig. 1a), dense branch morphology (DBM, Fig. 1b), and dendrite (Fig. 1c) corresponding to concentrations from low to high. This result indicates that the concentration of silver ions has an important effect on the morphology transform of silver trees from LF to DBM and even to dendrite. Between two morphologies, there is no clear boundary, and the transform is gradual, such as LF to DBM, with the concentration increasing, the density of LF morphology became higher and higher, and gradually changed to DBM shape.

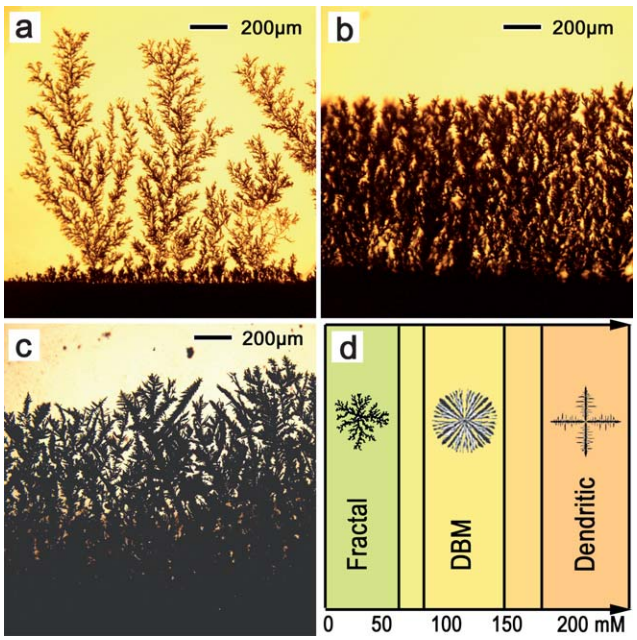

Fig. 1 Optical micrographs of hierarchical silver crystals grown on a zinc plate at different silver ion concentrations: (a) 30 mM, (b) 100 mM, and (c) 200 mM. (d) Morphology diagram in coordinates.

The micro-structure of the LF, DBM and dendrite silver trees was investigated by field-emission scanning electron microscopy (FE-SEM) and transmission electron microscopy (TEM). The SEM and TEM images of LF, DBM and dendrite silver trees prepared at concentrations of 30 mM, 100 mM, and 200 mM are shown in Fig. 2a–c and S2a–c† respectively. In Fig. 2a and S2a†, at a low concentration, the silver atoms are deposited randomly on a zinc plate and typical fractal morphology is formed. When the concentration increases to 100 mM, small dendrites begin to appear and the morphology density increases obviously (Fig. 2b and S2b†). Compared with LF trees prepared at 30 mM, the branches of DBM trees became much thinner and the density became much higher. When the concentration increases to 200 mM, the morphology transformed to uniform dendrite (Fig. 2c and S2c†). Compared with DBM, the branches of the dendrite became thicker and their density became lower. Electron energy dispersive X-ray (EDX) spectra and XRD patterns of the silver trees grown on a zinc plate at 100 mM concentration were measured. There are totally three elements: O, Zn and Ag (Fig. S3†). The signal of O and Zn may come from the zinc plate. The zinc plate surface should have been oxidized in an aqueous solution. The XRD patterns are matched very well with the diffraction from zinc crystal and silver crystal (Fig. S4†). For the silver crystal, the diffraction peaks are well indexed to (111), (200), (220)

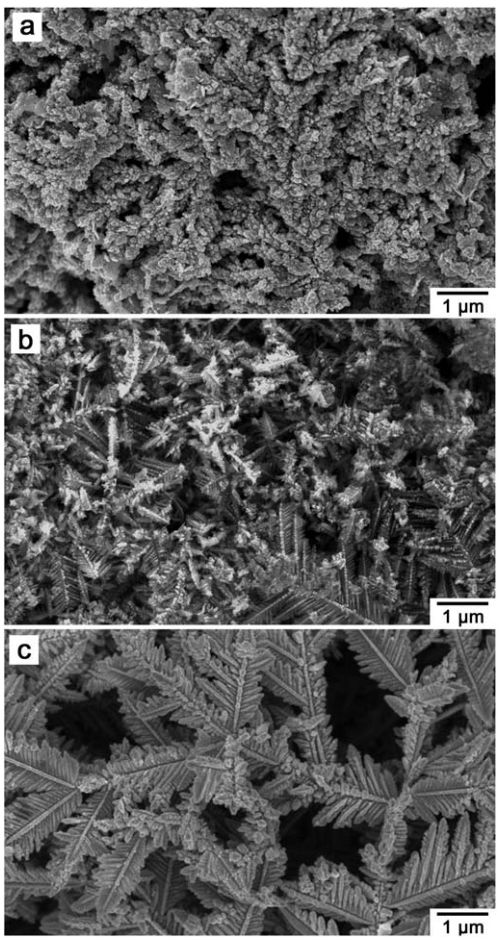

Fig. 2 FE-SEM images of silver hierarchical crystals grown on a zinc plate at different silver ion concentrations: (a) 30 mM, (b) 100 mM, and (c) 200 mM.

and (311) diffraction of standard face-centered cubic silver (JCPDS file no. 04-0836). The EDX spectrums and XRD patterns of the silver trees grown at 30 mM and 200 mM concentrations have similar results.

Because the concentration has an important effect on the morphology transforming of hierarchical silver crystals, the concentration profile near the silver crystal surface was *in situ* monitored using a Michelson interferometer. During the reaction, the silver ions at the reaction surface would be reduced to form atoms, and the concentration of silver ions was consumed. The silver ions in the bulk solution far from the reaction surface would diffuse toward the reaction surface, and thus a diffusion layer would be formed near the reaction surface. The concentration of silver ions was gradually changing in the diffusion layer and could be monitored by a Michelson interferometer.[39] The inset of Fig. 3a shows the interference fringe map of the diffusion layer measured by a Michelson interferometer and recorded by a CCD camera. The interference fringes change to curves in the area of the diffusion layer because of concentration change. The thicknesses of the diffusion layer (δ) at different concentration solutions were measured and shown in Fig. 3a. The thickness of the diffusion layer decreases dramatically with increasing concentration. All of the thicknesses were measured from interference fringes recorded at the reaction time of 60 s. At the first reaction stage, the concentration profile was not stable, and after 40 s, it gradually became stable. Fig. 3b shows the concentration profile recorded at different reaction times in a 30 mM silver ion solution and the inset of Fig. 3b shows the change of thickness *vs.* reaction time correspondingly. After 40 s of reaction time, the concentration profile became stable and the thickness of the diffusion layer kept constant. Miyashita and co-workers reported that in a DLA growth system, the thickness of the diffusion layer (δ) and the growth velocity (V) of the fractal trees can be described by following equations:[40]

$$V \approx c^{\alpha} \tag{3}$$

$$\delta \approx c^{\beta} \tag{4}$$

Here, c is the concentration of silver ions, α and β are constants depending on the reaction system, such as the normal space dimension and fractal dimension of silver trees. Fig. 3a shows that experiment data and theory curve are matched very well when β is -0.5.

Fig. 4a shows the growth velocities of silver trees on a zinc plate at different silver ions concentrations. With the concentration increasing, the growth velocity of silver trees increased dramatically. When the zinc plate was replaced with a copper plate, a similar result was obtained. Fig. 4b shows the growth velocity of silver trees on a copper plate. Comparing Fig. 4a with 4b, it shows that the reaction of the zinc plate is much faster than the copper plate, which is due to the different redox potentials between copper and zinc. Although the growth velocities are different for copper and zinc, they both can be described by eqn (1). When α is 1.5, both of the velocities of silver trees on the zinc plate and copper plate are matched very well with the theory curve.

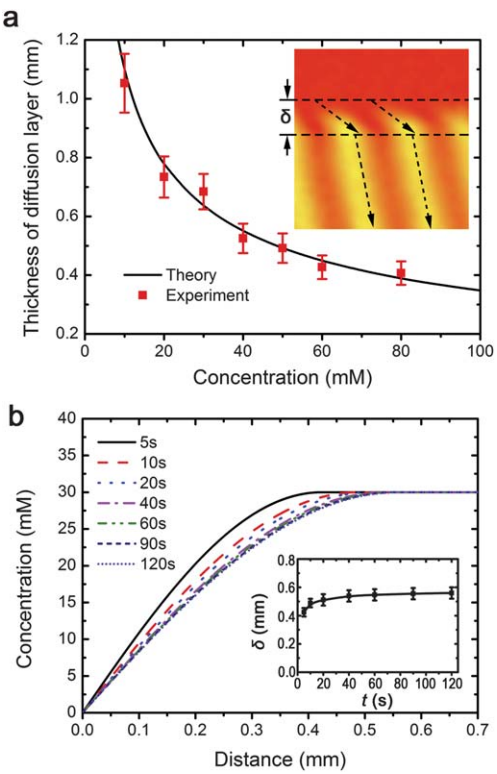

Fig. 3 (a) The thickness of the diffusion layer near reaction surface measured using a Michelson interferometer at different silver ion concentration solutions. Inset was the curved interference fringes near reaction surface monitored by a Michelson interferometer and recorded by a CCD camera. (b) Variation of the concentration profile near reaction surface with the reaction time increasing in a 30 mM silver ion concentration system. Inset shows the thickness changing of the diffusion layer (δ) *vs.* reaction time (t).

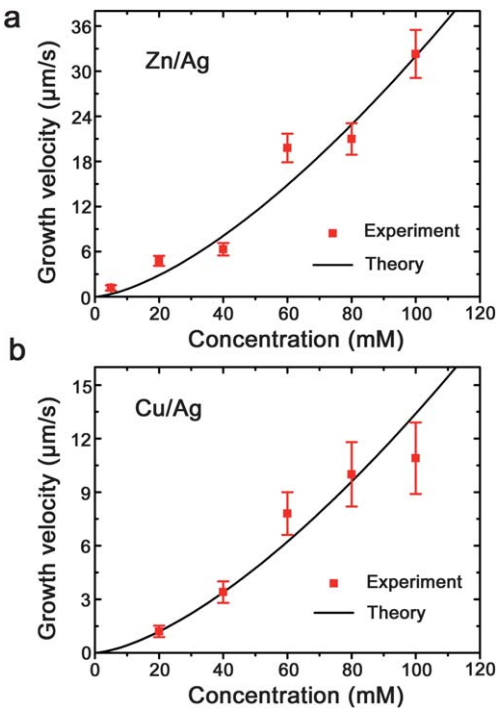

Fig. 4 The growth velocity of hierarchical silver trees *vs.* silver ion concentrations for (a) Zn plate and $AgNO_3$ (aq.) and (b) Cu plate and $AgNO_3$ (aq.) reaction system.

Based on the DLA model, people have simulated the forming of fractal morphology using the Monte Carlo method.[30] The simulation result shows that the morphology is decided by aggregation particles' walking. When the particles perform a random walking before aggregation, the final morphology will be LF; when the particles perform an anisotropic walking, the final morphology will be DBM. This result disclosed that the competition between random and anisotropic growth decided the morphology transforming from LF to DBM. However what decides the random and anisotropic growth in the experimental system is still not studied clearly. Here we think the concentration profile near the silver crystal performs an important effect. A schematic diagram of the effect of concentration profiles on the silver trees morphology transformation is presented in Fig. 5. Fig. 5a shows, at low concentration, the thickness of the diffusion layer is very thick, the silver ions in bulk solution need long times to diffuse to the reaction surface. As long as the silver ion reaches the reaction surface, it will be reduced immediately. Thus the concentration at the reaction surface is zero and there is competition for silver ions between branches of silver trees. The higher branches are easier to gain silver ions and grow more quickly than lower silver trees, and the growth of short branches is inhibited, thus LF morphology is formed. Fig. 5b shows when the concentration increases, the thickness of the diffusion layer decreases, there are more silver ions diffusing to the reaction surface in a certain time and more branches can gain silver ions to grow up. Thus the density of the morphology increases and DBM morphology is formed. Fig. 5c shows, with the concentration increasing further, more silver ions than the reaction needed are diffused to the reaction surface. The concentration is not zero at the reaction surface. The tips of silver trees are plugged into a higher concentration area, and they are easier to grow up at higher concentration conditions.

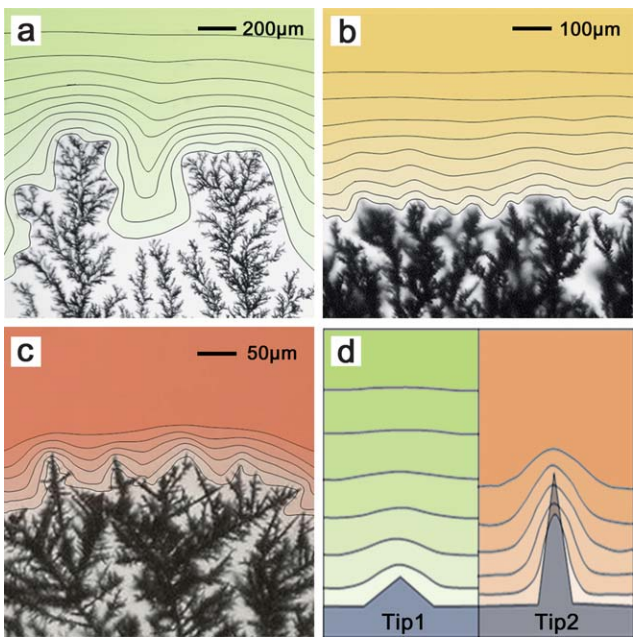

Fig. 5 Schematic representation to describe the effect of concentration profiles on the morphologies of silver hierarchical trees in different concentration solutions. The concentrations of bulk solutions were (a) 30 mM, (b) 100 mM, and (c) 200 mM. (d) Schematic drawing of two different growth modes of silver crystals induced by different concentration profiles.

Fig. 5d shows two crystal growth modes induced by different concentration profiles: one is diffusion limited aggregation (DLA), the other is reaction limited growth (RLG).[10] At a low concentration, the silver trees are dominated by DLA mode growth (Tip 1). At a high concentration, the growth is dominated by RLG mode (Tip 2). The former, DLA model, has been widely studied by many people, which can successfully explain the fractal morphology forming and transforming. In the later, RLG mode, there are more silver ions at the reaction surface than the reaction needed, the growth of silver trees is no longer limited by the diffusion of silver ions, but limited by the reaction. The reaction velocity on tips is accelerated by two factors: firstly the tips protuberate at a high concentration area. For a chemical reaction in solution, the reaction velocity is increased with concentration increase. Secondly the tips have higher activity than planes.[41] Thus the tips grow much more quickly than other parts and this protuberated growth induced dendrite morphology forming. According to the studies of Despic *et al.*,[42] the protuberance height and reaction time (t) can be expressed as:

$$Y(x,t) = Y_0\exp(t/\tau) \quad (5)$$

where Y_0 is the origination height at $t = 0$, τ is the induction time which in certain conditions can be written as:

$$\tau \approx \delta^2/c_m \quad (6)$$

Here c_m is the concentration of bulk solution. Depending on these two equations, at a higher concentration solution, the thickness of the diffusion layer decreases dramatically and the concentration increases. The tips will grow more quickly to protuberate into a high concentration area. Thus an anisotropic growth induced by the concentration profile is appeared in a high concentration solution and dendrite morphology is formed.

To summarize, in this study, the silver hierarchical crystals with different morphologies are synthesized in an electrochemical cell using the Zn/$AgNO_3$ (aq.) replacement reaction system. A morphological transition from fractal style to the typical DBM and even to dendritic pattern is observed as silver ion concentration increases. A morphology diagram is developed for depicting the observation here, which demonstrates that the evolution of the morphologies is a function of concentration. The concentration profile near the reaction surface was measured by a Michelson interferometer and its effect on morphology transform of silver trees was investigated. There are two different growth modes for the silver trees growth induced by the concentration profile: one is DLA, the other is RLG. The typical fractal morphology is formed by DLA mode and the dendritic morphology is formed by RLG mode.

Acknowledgements

This work was supported by the National Basic Research Program of China (No. 2010CB635101), the Tengfei Talent project of Xi'an Jiaotong University, the Fundamental Research Funds for the Central Universities (No. 08142008), National Science Foundation of China (NSFC No. 50871080 and 50901056).

References

1 Z. M. Peng and H. Yang, *Nano Today*, 2009, **4**, 143–164.
2 J. P. Xiao, Y. Xie, R. Tang, M. Chen and X. B. Tian, *Adv. Mater.*, 2001, **13**, 1887–1891.
3 B. Lim, M. Jiang, T. Yu, P. H. C. Camargo and Y. Xia, *Nano Res.*, 2010, **3**, 69–80.
4 Z. M. Peng and H. Yang, *Nano Res.*, 2009, **2**, 406–415.
5 B. Lim, M. J. Jiang, P. H. C. Camargo, E. C. Cho, J. Tao, X. M. Lu, Y. M. Zhu and Y. A. Xia, *Science*, 2009, **324**, 1302–1305.
6 J. Fang, S. Du, S. Lebedkin, Z. Li, R. Kruk, M. Kappes and H. Hahn, *Nano Lett.*, 2010, **10**, 5006–5013.
7 Y. J. Song, Y. Yang, C. J. Medforth, E. Pereira, A. K. Singh, H. F. Xu, Y. B. Jiang, C. J. Brinker, F. van Swol and J. A. Shelnutt, *J. Am. Chem. Soc.*, 2004, **126**, 635–645.
8 W. R. Zhu, X. P. Zhao and J. Q. Guo, *Appl. Phys. Lett.*, 2008, **92**, 241116.
9 Y.-J. Song, J.-Y. Kim and K.-W. Park, *Cryst. Growth Des.*, 2008, **9**, 505–507.
10 H. J. You, J. X. Fang, P. Kong and B. J. Ding, *Rare Metal Mater. Eng.*, 2008, **37**, 1042–1045.
11 S. D. Sun, C. C. Kong, D. C. Deng, X. P. Song, B. J. Ding and Z. M. Yang, *CrystEngComm*, 2011, **13**, 63–66.
12 M. Aizawa, A. M. Cooper, M. Malac and J. M. Buriak, *Nano Lett.*, 2005, **5**, 815–819.
13 J. X. Fang, H. J. You, P. Kong, Y. Yi, X. P. Song and B. J. Ding, *Cryst. Growth Des.*, 2007, **7**, 864–867.
14 X. Q. Wang, K. Naka, H. Itoh, S. Park and Y. Chujo, *Chem. Commun.*, 2002, 1651–1651.
15 H. Imai, H. Nakamura and T. Fukuyo, *Cryst. Growth Des.*, 2005, **5**, 1073–1077.
16 Y. Zhou, S. H. Yu, C. Y. Wang, X. G. Li, Y. R. Zhu and Z. Y. Chen, *Adv. Mater.*, 1999, **11**, 850–852.
17 V. Fleury, W. A. Watters, L. Allam and T. Devers, *Nature*, 2002, **416**, 716–719.
18 S. Z. Wang and H. W. Xin, *J. Phys. Chem. B*, 2000, **104**, 5681–5685.
19 Y. Socol, O. Abramson, A. Gedanken, Y. Meshorer, L. Berenstein and A. Zaban, *Langmuir*, 2002, **18**, 4736–4740.
20 M. Wang, W. J. P. Vanenckevort, N. B. Ming and P. Bennema, *Nature*, 1994, **367**, 438–441.
21 A. Nahal, J. Mostafavi-Amjad, A. Ghods, M. R. H. Khajehpour, S. N. S. Reihani and M. R. Kolahchi, *J. Appl. Phys.*, 2006, **100**, 053503.
22 Y. Sawada, A. Dougherty and J. P. Gollub, *Phys. Rev. Lett.*, 1986, **56**, 1260–1263.
23 S. Lv, H. Suo, H. Wang, C. Wang, J. Wang, Y. Xu and C. ZHao, *Solid State Sci.*, 2010, **12**, 1287–1291.
24 C. Yan and D. Xue, *Cryst. Growth Des.*, 2008, **8**, 1849–1854.
25 H. Rashid and T. K. Mandal, *J. Phys. Chem. C*, 2007, **111**, 16750–16760.
26 H. Brune, C. Romainczyk, H. Roder and K. Kern, *Nature*, 1994, **369**, 469–471.
27 J. X. Fang, H. J. You, C. Zhu, P. Kong, M. Shi, X. P. Song and B. J. Ding, *Chem. Phys. Lett.*, 2007, **439**, 204–208.
28 J. A. Corno, J. Stout, R. Yang and J. L. Golet, *J. Phys. Chem. C*, 2008, **112**, 5439–5446.
29 J. S. Langer, *Science*, 1989, **243**, 1150–1156.
30 V. A. Bogoyavlenskiy and N. A. Chernova, *Phys. Rev. E: Stat. Phys., Plasmas, Fluids, Relat. Interdiscip. Top.*, 2000, **61**, 1629–1633.
31 H. M. Zheng, R. K. Smith, Y. W. Jun, C. Kisielowski, U. Dahmen and A. P. Alivisatos, *Science*, 2009, **324**, 1309–1312.
32 R. L. Penn and J. F. Banfield, *Science*, 1998, **281**, 969–971.
33 Z. M. Peng, H. J. You and H. Yang, *ACS Nano*, 2010, **4**, 1501–1510.
34 F. Huang, H. Z. Zhang and J. F. Banfield, *Nano Lett.*, 2003, **3**, 373–378.
35 J. X. Fang, B. J. Ding and X. P. Song, *Cryst. Growth Des.*, 2008, **8**, 3616–3622.
36 S. Cheong, J. Watt, B. Ingham, M. F. Toney and R. D. Tilley, *J. Am. Chem. Soc.*, 2009, **131**, 14590–14595.
37 J. X. Fang, H. J. You, P. Kong, B. J. Ding and X. P. Song, *Appl. Phys. Lett.*, 2008, **92**, 143111.
38 Y. G. Sun and Y. N. Xia, *J. Am. Chem. Soc.*, 2004, **126**, 3892–3901.
39 H. J. You, J. X. Fang, F. Chen, C. Zhu, X. P. Song and B. J. Ding, *Chem. Phys. Lett.*, 2008, **465**, 131–135.
40 S. Miyashita, Y. Saito and M. Uwaha, *J. Cryst. Growth*, 2005, **283**, 533–539.
41 S. C. Tsang, N. Cailuo, W. Oduro, A. T. S. Kong, L. Clifton, K. M. K. Yu, B. Thiebaut, J. Cookson and P. Bishop, *ACS Nano*, 2008, **2**, 2547–2553.
42 A. R. Despic, J. Diggle and J. O. M. Bockris, *J. Electrochem. Soc.*, 1968, **115**, 507–508.